



Development of non-stationary temperature duration frequency curves for Indian mainland

Meera G. Mohan^{1,2} · Adarsh S.^{1,2}

Received: 30 April 2022 / Accepted: 14 August 2023 / Published online: 26 August 2023
© The Author(s), under exclusive licence to Springer-Verlag GmbH Austria, part of Springer Nature 2023

Abstract

Extreme temperature events are one of the most serious threats resulting from climatic change across the globe. Quantifying the intensity, duration, and frequency of temperature extremes is of huge societal and scientific interest. Recent evidence in climate change challenges the stationarity assumption conventionally followed while performing temperature-duration-frequency (TDF) analysis. India has distinct climate zones and topography, distributing climate threats unevenly. In this study, stationary (S) and non-stationary (NS) TDF analysis for India and its seven temperature homogenous areas is performed using a gridded ($1^\circ \times 1^\circ$) daily maximum temperature dataset from 1951 to 2019. Time is employed as a covariate to incorporate linear, quadratic, and exponential trends in the location and/or scale parameters of the generalized extreme value distribution to demonstrate the impact of non-stationarity in developing TDF curves. According to the findings, NS TDF models provide a better fit to the dataset when compared to the S TDF model. More than 55% of the grid points have NS Model-1, viz., location parameter linearly varying with time, as the best-fit model. In contrast to their stationary counterparts, NS temperature return levels were consistently higher across all return periods. Furthermore, temperature homogenous zones in the North-West, North Central, and Interior Peninsula are more susceptible to temperature rises beyond 45°C . While envisioning long-term solutions in a changing climate scenario, considering non-stationarity significantly improved the accuracy of TDF curves. This will indeed support more robust predictions, which will ultimately aid in the mitigation of future extreme temperature events.

1 Introduction

Anthropogenic climate change has far-reaching consequences, one of which is a shift towards extreme weather events. According to the Intergovernmental Panel on Climate Change (IPCC 2013), it is anticipated that the intensity, duration, frequency, and extent of climate extremes (e.g., heat waves, droughts, cyclones, and floods) will increase across the globe. Air temperature is a crucial element of the weather system; therefore, it is highly important to investigate and analyze the temporal-spatial variability patterns of temperature extremes brought on by climate change on a

regional, national, and global scale (Khan et al. 2015). The latest IPCC report (IPCC 2021) states that the world will reach or exceed a 1.5°C temperature rise within the next two decades. Extreme temperatures have an undesirable influence on human health, man-made infrastructure, and natural ecosystems when they persist for extended periods of time. Researchers have been interested in temperature extremes ever since climate change started ruling the Earth. The previous studies on temperature extremes include analysis of Australian heatwaves (Perkins and Alexander 2013), changes in the frequency of warm and cold exceedances in India (Dash and Mangain 2011), trends in heatwave indices of India (Kothawale et al. 2010; Rohini et al. 2016) and Pakistan (Khan et al. 2019), and changes in maximum, minimum, and mean temperatures of Iran (Ghasemi 2015). In the last few decades, some studies have revealed that climatic and meteorological records exhibit some type of non-stationarity, such as trends and shifts (Douglas et al. 2000; Yan et al. 2002; Tank and Können 2003).

Frequency analysis (FA) is a conventional tool for exploring the behavior of hydro-meteorological variables like

✉ Adarsh S.
adarsh_lce@yahoo.co.in

Meera G. Mohan
meeragmohan90@gmail.com

¹ TKM College of Engineering, Kollam, Kerala PIN-691005, India

² APJ Abdul Kalam Technological University, Thiruvananthapuram, Kerala, India

rainfall, flood, drought, temperature, and wind speed (Khaliq et al. 2005). It can be carried out by developing time series of extreme variables using two approaches, namely, the annual maximum series (AMS) and the peak over threshold (POT) series. In the case of AMS, there is only one value per year, while in the case of POT series, there may be more than one value per year as it considers all values above a particular threshold. The main difficulties faced while incorporating the POT method are ensuring independence of the extracted data, selection of an appropriate threshold value, and additional uncertainty issues such as sample size variation (i.e., average events per year are not fixed) and effects of data extraction time scale (e.g., minute, hourly, daily, or monthly scales). FA is carried out to establish a relationship curve between intensity, duration, and frequency of a chosen variable and to quantify the return level intensities for various return periods. These curves are developed based on historical time series datasets for specific durations by fitting a suitable theoretical probability distribution (Agilan and Umamahesh 2017). The most commonly studied FA are the rainfall intensity-duration-frequency (IDF) (Mondal and Mujumdar 2015; Agilan and Umamahesh 2017; Ray and Goel 2019), discharge-duration-frequency (QDF) (Javelle et al. 2002; Onyutha and Willems 2013; Renima et al. 2018), and drought severity-duration-frequency (SDF) (Shiau and Modarres 2009; Sung and Chung 2014; Rahmat et al. 2015; Adarsh et al. 2018). However, research on temperature-duration-frequency (TDF) curves, which map out the relationship between intensity of temperature events of different durations to their frequencies, is sparse. TDF curves prove to be useful tools for the analysis of heat extremes (Ouarda and Charron 2018).

Conventionally, the TDF relationship is developed based on stationary probabilistic distributions; i.e., the distribution parameters remain constant with time. This assumption of stationarity does not hold true as the characteristics of extreme temperature events vary with respect to time as a result of climate change and variability. It demands the incorporation of dynamic behavior in distribution parameters, paving the way for non-stationarity. Non-stationary probabilistic distributions consider the distribution parameters to vary with respect to one or more covariates, namely, time and climatic oscillations (Coles 2001). Assuming that the properties of the probability distribution of extreme heat occurrences are invariant with time, Khaliq et al. (2005) were the first to create the notion of TDF curves. The study was conducted at four stations in the southern Quebec region of Canada. This work was further extended to the non-stationary concept of TDF curves by Ouarda and Charron (2018) for six stations in Quebec, Canada. Goodness of fit was found to increase when a non-stationary strategy was used in conjunction with covariates representing climatic variability. Mazdiyasnani et al. (2019) constructed heat wave

IDF curves to attribute changes in heat waves to anthropogenic warming by comparing global climate model simulations with and without anthropogenic emissions for Los Angeles, California.

In the past decades, many studies have addressed the changes in temperature conditions and their extremes in India, as this is the major driver behind the climatic changes (Kothawale and Rupa Kumar 2005; Sonali and Nagesh Kumar 2013; Vinnarasi et al. 2017; Roy 2019). As far as India is concerned, heatwaves have caused 1300, 2042, 3054, and 2248 deaths in the years 1988, 1998, 2003, and 2015, respectively (Ratnam et al. 2016; Mazdiyasnani et al. 2017). A significant increase in the frequency, persistence, and spatial coverage of extreme temperature events has been reported by researchers (Raghavan 1966; De and Mukhopadhyay 1998; Pai et al. 2004; De et al. 2005) in the years 1991–2000 when compared with the previous two decades. The study by Rao et al. (2005) concluded that 80% of stations in Peninsular India and 40% of stations in Northern India display a rise in trend in extreme temperature days for the period 1971–2000. The northern, north-central, and north-eastern parts of India experience high temperatures, resulting in heat waves during the pre-monsoon (March–May) and summer (April–June) seasons. There has been a dominant rise in temperature (during 1969–2013) over continental India, resulting in an increase in the frequency of occurrence of extreme temperature events (Kothawale et al. 2010; Revadekar et al. 2012; Oza and Kishtawal 2015). Some researchers stated that there was an increasing trend in the frequency, average duration, and maximum duration during the period 1961–2013 over the north-west and southeast regions of India (Rohini et al. 2016; Singh et al. 2020). Even though Indian researchers have analyzed heatwaves with the help of daily maximum temperatures based on various aspects, studies for developing a relationship between their intensity, duration, and frequency are quite ignored, unlike hydrological studies. Recently, Devi et al. (2021) conducted a stationary TDF analysis over two megacities in India, Delhi (north) and Bengaluru (south), using the daily maximum temperatures with two distributions, i.e., Gumbel's extreme value type 1 and log Pearson type III, for the period of 1969–2016. The TDF was also used for the prediction of the maximum temperature for the 2 hottest years in India, i.e., 2012 and 2015, and it was compared with the observed maximum temperature. To the best of our knowledge, no studies focusing on developing TDF curves in a NS framework have been addressed for the whole of India.

Hence, this study will be the first to demonstrate NS TDF analysis for India and its seven temperature-homogeneous regions using the daily maximum gridded temperature dataset. The TDF relationship is developed with both stationary (S) and non-stationary (NS) generalized extreme value (GEV) models. Seven NS models were developed using

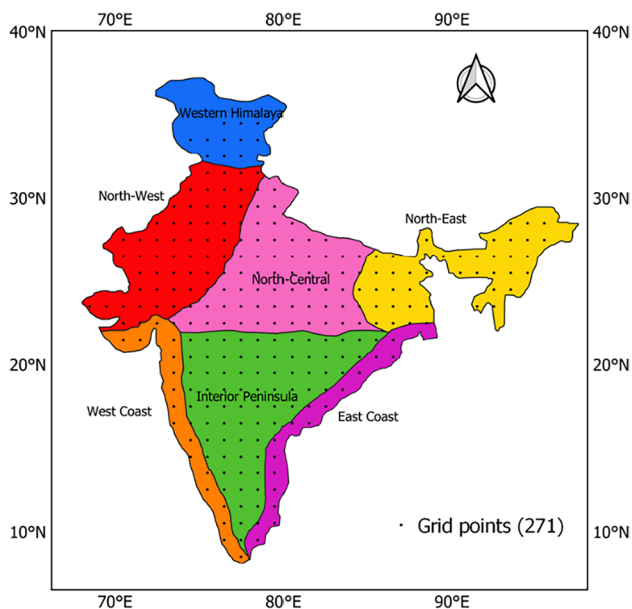


Fig. 1 Seven temperature-homogeneous regions of India

location and scale parameters that can be considered stationary or can depend linearly, quadratically, or exponentially on time. The best-fit model is chosen based on the Akaike information criterion. The objectives of the study are (i) to develop S and NS TDF curves for all the grid points covering India, (ii) to compare S and NS return level temperatures for quantifying the percentage variation, and (iii) to analyze the return level temperature variations in each temperature-homogeneous region of India for different durations and return periods.

2 Study area and data processing

India is the seventh-largest country in the world and ranks third in the contribution of greenhouse gas emissions in the world. Between 1901 and 2018, the average temperature in India rose by 0.7°C, significantly altering the country’s weather patterns. The Indian Institute of Tropical Meteorology at Pune has classified the whole of India into seven temperature-homogeneous regions, namely, the North West (NW), Western Himalayas (WH), West Coast (WC), East Coast (EC), North East (NE), North Central (NC), and

Interior Peninsula (IP), as shown in Fig. 1, on the basis of spatial and temporal variations of surface air temperatures across the country.

High-resolution gridded (1° latitude × 1° longitude) daily maximum temperature data for India is available from the Indian Meteorological Department (IMD), Pune, for a period of 69 years from 1951 to 2019 (Srivastava et al. 2009). The raw data was processed and cleaned with the goal of removing grid points that were lying outside India and had null values. A total of 271 grid points were finally obtained, spreading out throughout India and its seven temperature-homogeneous regions. The annual maximum of multi-day averages of daily maximum temperatures was extracted over 7 durations (1 day, 2 days, 4 days, 6 days, 8 days, 10 days, and 12 days) for each grid point.

The Mann-Kendall (MK) trend test (Mann 1945; Kendall 1975) was carried out to detect the presence of non-stationarity in the annual maximum gridded temperature dataset for all durations. A normalized test statistic, Z, was used to statistically quantify the significance of the trend at 95% confidence level. The positive values of z represent an increasing trend, while negative values indicate a decreasing trend. If the MK test statistic of the temperature time series is greater than ± 1.96, then it represents a significant increasing or decreasing trend with a non-stationary behavior. The trend test was conducted as a preliminary analysis to confirm the presence of non-stationarity for the whole of India to proceed with the S and NS TDF modeling.

3 Methodology

3.1 Stationary and non-stationary extreme value modeling

Extreme value theory (EVT) is a framework for dealing with the stochastic behavior of extreme events and is appropriate for analyzing risks associated with climate extremes (Katz et al. 2002; Coles 2001). The GEV distribution is a continuous probability distribution developed within EVT commonly used to estimate and analyze extremes (Gumbel 1958). Consider an annual maximum series of *n* independent and identically distributed random variables *x*₁, *x*₂, ..., *x*_{*n*}. The annual maximum series converges to the GEV distribution, and the cumulative distribution function is given by Eq. 1.

$$F(x, \mu, \sigma, \xi) = \begin{cases} \exp \left\{ - \left[1 + \xi \left(\frac{x - \mu}{\sigma} \right) \right]^{-1/\xi} \right\}, & \sigma > 0, 1 + \xi \left(\frac{x - \mu}{\sigma} \right) > 0, \xi \neq 0 \\ \exp \left\{ - \exp \left[- \left(\frac{x - \mu}{\sigma} \right) \right] \right\}, & \sigma > 0, \xi = 0 \end{cases} \tag{1}$$

where μ , σ , and ξ are the location, scale, and shape parameters of the GEV distribution, respectively. The location parameter (μ) determines the shift of the distribution to the right or left on the horizontal axis. It is mainly associated with the mean of the distribution. The scale parameter (σ) characterizes the variance or spread of the distribution. It usually stretches or squeezes the distribution. The shape parameter (ξ) defines the shape of the distribution, and it depends on skewness and kurtosis. It is usually kept constant because it rarely varies as a function of time (Coles 2001). The GEV distribution was used to develop both the S and NS TDF models. In the S TDF model, the location, scale, and shape parameters are assumed to be constant, while for NS TDF models, location and scale parameters are considered to vary linearly and non-linearly with respect to time, whereas the shape parameter is kept constant. The S model and best NS models among the linear, quadratic, and exponential relationships are shown in Table 1.

3.2 Parameter estimation

There are several methods to estimate the distribution parameters, such as maximum likelihood estimation (MLE) (Smith 1985), probability weighted moment (Hosking et al. 1985), L-moments (Hosking 1990), method of moments (Madsen et al. 1997), and generalized maximum likelihood estimators (El Adlouni et al. 2007). The most commonly used method is the MLE because it can be easily extended to NS models (Coles 2001), and the same is used in this study for estimating S and NS GEV parameters. Let the values $X = x_1, x_2, \dots, x_n$ be the n years of the annual maximum series. The log likelihood is derived from Eqs. (2) and (3).

For $\xi \neq 0$,

$$\log L(\mu, \sigma, \xi|X) = -n \log \sigma - \left(1 + \frac{1}{\xi}\right) \sum_{i=1}^n \log \left[1 + \xi \left(\frac{x_i - \mu}{\sigma}\right)\right] - \sum_{i=1}^n \left[1 + \xi \left(\frac{x_i - \mu}{\sigma}\right)\right]^{-1/\xi}, 1 + \xi \left(\frac{x_i - \mu}{\sigma}\right) > 0 \tag{2}$$

For $\xi=0$,

$$\log L(\mu, \sigma|X) = -n \log \sigma - \sum_{i=1}^n \left(\frac{x_i - \mu}{\sigma}\right) - \sum_{i=1}^n \exp \left[-\left(\frac{x_i - \mu}{\sigma}\right)\right] \tag{3}$$

For the non-stationary case, the location and scale parameters in the above equations are replaced with the corresponding equations in Table 1 based on the model application. Maximization of Eqs. (2) and (3) with respect to the parameter vector (μ, σ, ξ) leads to the maximum likelihood estimate (Coles 2001).

3.3 Determination of the best model

The Akaike information criterion (AIC) is a goodness-of-fit measure used for evaluating how well a model fits the data it was generated from. In this study, AIC is used to compare the S and NS models to determine the best suited model. The model with the smallest AIC value is considered to be the best possible fit for the temperature data. AIC determines the relative information value of the model using the maximum likelihood estimate and the number of parameters (independent variables) in the model as given in Eq. (4).

$$AIC = 2K - 2 \ln(L) \tag{4}$$

where K is the number of independent variables used and L is the log-likelihood estimate.

3.4 Estimation of return level temperatures

The estimation of return level and return period is mainly carried out in hydrology and climate studies to assess the risk (probability of occurrence) of extremes. Return period (RP), also known as recurrence interval, provides an estimate of the likelihood of any event to occur in a year. RPs convey the risks of events more effectively than simply stating their probabilities.

The estimation of the stationary temperature return level is very simple as the distribution parameters are assumed to be constant. Unlike stationary models, non-stationary temperature return levels are computed using the model parameters of the best-fit NS model identified in Section 3.3. This is because the location and scale parameters are considered to be time-variant. A representative value of the time-varying effective return level (Cheng et al. 2014; Agilan and Umamahesh 2017), i.e., the quantile corresponding to the 95th percentile of the time-varying location (Eq. (5)) and scale parameter (Eq. (6)), is considered in this study.

Table 1 Development criteria of stationary and non-stationary TDF models

Model	Model parameters
Stationary	μ, σ, ξ
NS Model-1	$\mu_t = \mu_0 + \mu_1 \text{Time}, \sigma, \xi$
NS Model-2	$\mu, \sigma_t = \sigma_0 + \sigma_1 \text{Time}, \xi$
NS Model-3	$\mu_t = \mu_0 + \mu_1 \text{Time}, \sigma_t = \sigma_0 + \sigma_1 \text{Time}, \xi$
NS Model-4	$\mu, \sigma_t = \exp(\sigma_0 + \sigma_1 \text{Time}), \xi$
NS Model-5	$\mu_t = \mu_0 + \mu_1 \text{Time}, \sigma_t = \exp(\sigma_0 + \sigma_1 \text{Time}), \xi$
NS Model-6	$\mu_t = \mu_0 + \mu_1 \text{Time} + \mu_2 \text{Time}^2, \sigma, \xi$
NS Model-7	$\mu, \sigma_t = \sigma_0 + \sigma_1 \text{Time} + \sigma_2 \text{Time}^2, \xi$

$$\hat{\mu}_{95} = Q_{95}(\hat{\mu}_{t1}, \hat{\mu}_{t2}, \dots, \hat{\mu}_{tm}) \tag{5}$$

$$\hat{\sigma}_{95} = Q_{95}(\hat{\sigma}_{t1}, \hat{\sigma}_{t2}, \dots, \hat{\sigma}_{tm}) \tag{6}$$

The location and scale parameters estimated using Eqs. (5) and (6) are substituted in Eq. (7) to calculate the NS temperature return level, I (°C) at various return periods, T , in years (Coles 2001; Cheng et al. 2014).

$$I = \begin{cases} \hat{\mu} + \frac{\hat{\sigma}}{\xi} \left[\left(-\log \left(1 - \frac{1}{T} \right) \right)^{-\xi} - 1 \right], & \hat{\xi} \neq 0 \\ \hat{\mu} + \hat{\sigma} \left[-\log \left(-\log \left(1 - \frac{1}{T} \right) \right) \right], & \hat{\xi} = 0 \end{cases} \tag{7}$$

4 Results and discussions

In this study, the MK test was carried out for India for all 7 durations (1, 2, 4, 6, 8, 10, and 12 consecutive days) separately to identify the grid points that display a non-stationary behavior. The grid points are categorized into four classes: NS increasing trend ($z \geq 1.96$), NS decreasing trend ($z \leq -1.96$), increasing trend ($0 \leq z < 1.96$), and decreasing trend ($0 > z > -1.96$) for each

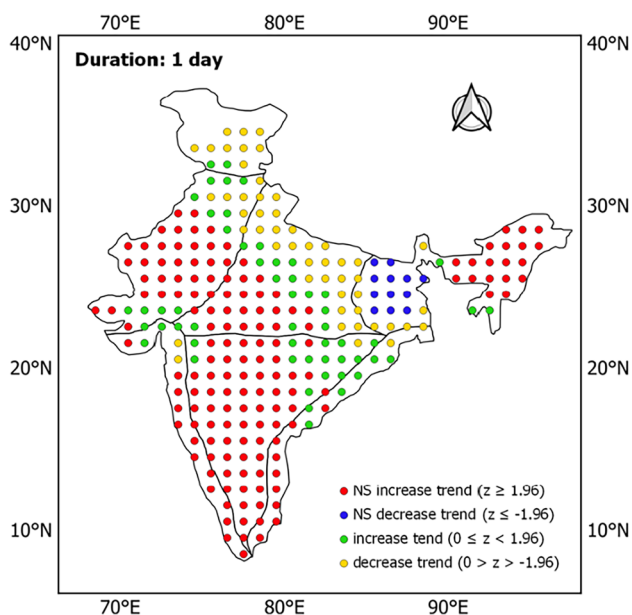


Fig. 2 Spatial representation of grid points with significant trend for 1-day duration

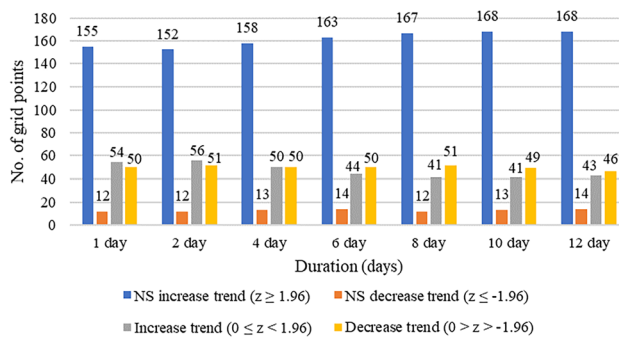


Fig. 3 Grid points with significant trend for different durations

duration. Figure 2 represents how the trend is distributed spatially along the grid points all over India for duration of 1 day. A bar chart representation of the number of grid points falling under each class for all durations is given in Fig. 3. It was found that more than 57% of the grid points have a significant non-stationary increasing trend for all durations. The significance of the non-stationary trend seemed to increase gradually, accounting to 62% for a 12-day duration. This necessitates the need to conduct NS TDF analysis in India.

TDF models were developed for both stationary and non-stationary cases to critically analyze, evaluate, and compare the results so obtained to communicate the exigency of considering non-stationarity in the future.

4.1 Overall analysis of best-fit models

The best-fit model for each temperature duration series was identified from the S and NS models using AIC values. Overall, 3 best models (NS Model-1, NS Model-6, and NS Model-4) are identified among the TDF models developed for 7 durations at 271 grid points spanning over India. The NS models vary based on location and scale parameters as they are conditional on time-bound covariates.

A detailed analysis of the percentage of grid points that fit each model for each duration is given in Table 2. It can be inferred that more than 55% of the grid points performed well for NS Model-1, i.e., location parameter linearly varying with respect to time, for all the durations. The second best-fit model is NS Model-6, i.e., location parameter varying quadratically with respect to time, with percentage of grid points varying in the range of 21 to 25% for each duration. The third one was NS Model-4, i.e., scale parameter exponentially varying with time, with percentage of grid points varying in the range of 10 to 15% for each duration. The number of grid points supporting NS Model-1 increased to 67% for the 12-day duration.

Table 2 Percentage of best-fit models for each duration for all grid points

NS models	Durations						
	1 day	2 days	4 days	6 days	8 days	10 days	12 days
NS Model-1	55%	55%	57%	60%	64%	67%	67%
NS Model-2	1%	1%	0%	0%	0%	0%	0%
NS Model-3	1%	1%	1%	1%	0%	0%	0%
NS Model-4	15%	14%	13%	10%	10%	10%	10%
NS Model-5	4%	4%	4%	3%	3%	1%	1%
NS Model-6	24%	25%	25%	25%	23%	21%	21%
NS Model-7	0%	0%	0%	0%	0%	0%	0%

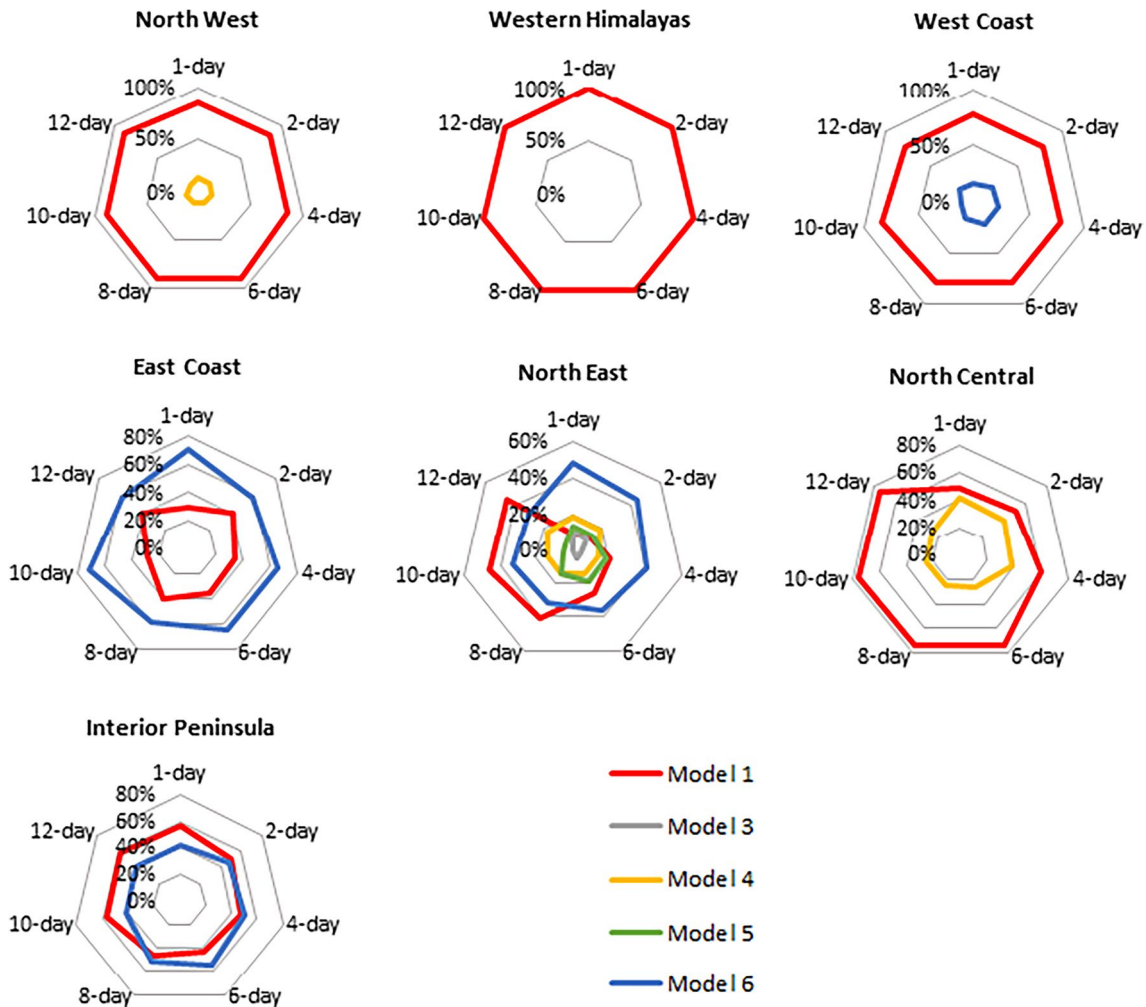


Fig. 4 Region-wise analysis of the best fitting models for different durations

4.2 Region-wise analysis of best-fit models

A temperature-homogeneous region-wise analysis was also carried out for a deeper understanding. Figure 4 represents the best-fit model for each duration for each temperature-homogeneous region. In the NW region, more than 84% of its grid points performed well for NS Model-1 for all

durations, while the remaining percentage of grid points performed well for NS Model-4. The best-fit model was NS Model-1 for all the grid points in the WH region for all durations. The WC region has more than 77% of its grid points supporting NS Model-1, while less than 23% of the grid points support NS Model-6 as the best-fit model. For the EC region, NS Model-6 exceeded NS Model-1 for majority

of its grid points for all durations. The grid points of the NE region belonged to a variety of various NS models, namely, NS Model-6, NS Model-1, NS Model-4, NS Model-5, and NS Model-3. NS Model-6 took the lead for shorter durations, and for durations beyond 6 days, NS Model-1 was the best-fit model. Less than 20% of the grid points had NS Model-4, NS Model-5, and NS Model-3 as the best-fit models. In the NC region, NS Model-1 and NS Model-4 shared almost equal contributions of grid points at 1-day and 2-day durations. Beyond 2-day duration, there is a significant increase in the percentage of grid points that functioned well for NS Model-1. The IP region has almost equal contributions to NS Model-1 and NS Model-6. NS Model-1 turns out to be more dominant for durations beyond 8 days. The geographical allocation of the best-fit NS models for entire India and its temperature-homogeneous regions for 1-day duration is shown in Fig. 5 as an example. The best-fit models for all other durations are spatially represented in the supplementary material (Figure S1). As mentioned earlier, it was found that different best-fit NS models were obtained for different durations for the same grid point. In general, it can be concluded that variation of location parameter linearly (NS Model-1) or quadratically (NS Model-6) with respect to time influences the grid points significantly.

4.3 Stationary and non-stationary TDF curves

To demonstrate the impacts of considering NS TDF models instead of the traditional S TDF models, TDF curves are plotted for both cases in the same graph. TDF curves are generally represented on graphs with the temperature

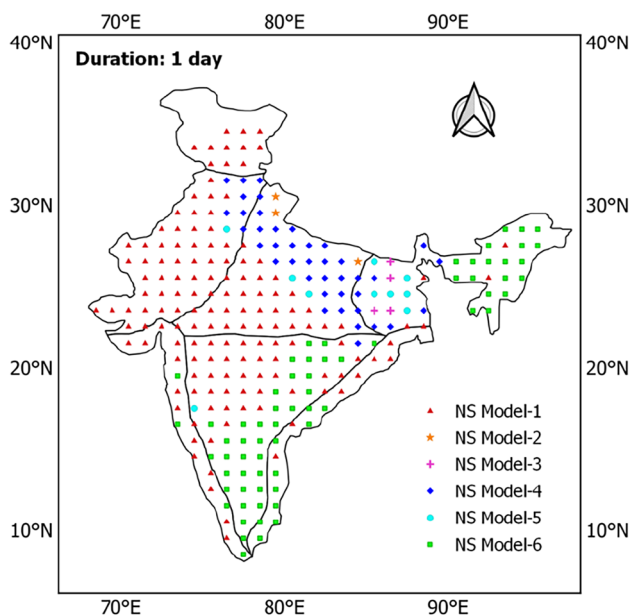


Fig. 5 Best-fit model of different grid points for 1-day duration

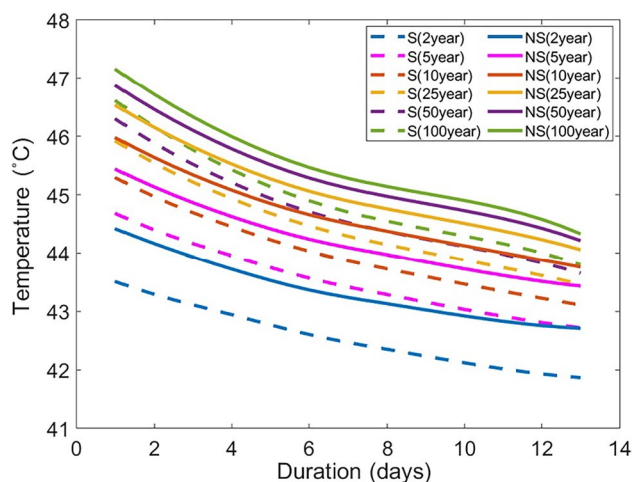


Fig. 6 Sand NS TDF curve for grid point 26.5° N x 70.5° E (Rajasthan-NW)

plotted against the duration, where each curve represents a return period (RP), say, 2 years, 5 years, 10 years, 25 years, 50 years, and 100 years in this study. Due to space constraints, one sample grid point in Rajasthan (26.5° N x 70.5° E) belonging to the NW homogenous region, which comprises the Indian desert, is considered a representative grid point in the study due to its prominent temperature. Figure 6 represents the S and NS TDF curves of this sample grid point. This figure illustrates the importance of considering time as a covariate when building TDF curves, as large discrepancies in quantiles are obtained for different RPs when compared to the stationary quantiles. For example, considering the sample grid point of Rajasthan (26.5° N x 70.5° E), the NS temperature return level of 1-day duration event with a 2-year RP is 44.42°C, whereas the same for the S model is 43.51°C, resulting in a difference of 0.91°C. TDF surfaces can be defined by representing them as 3D graphs of the temperature against the duration and the covariate, time. The same chosen grid point is used to represent the

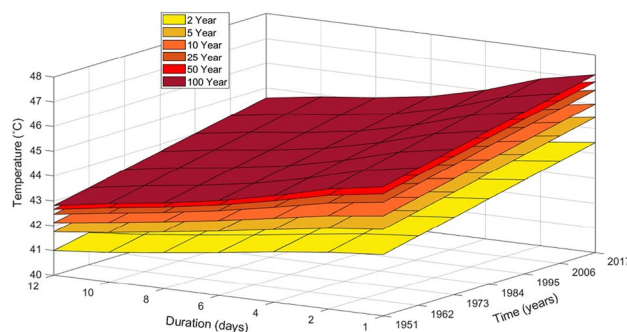


Fig. 7 NS TDF surfaces for grid point 26.5° N x 70.5° E (Rajasthan-NW)

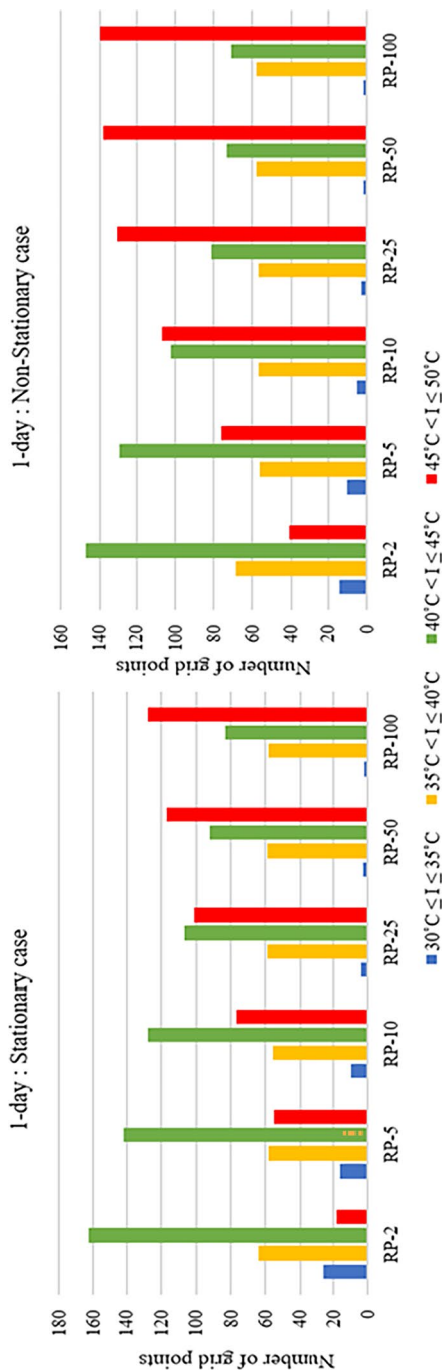


Fig. 8 Temperature variation of the grid points for 1-day duration

NS TDF surface in Fig. 7. The S and NS TDF curves and NS TDF surfaces for one grid point from each temperature-homogeneous region are shown in the supplementary material (Figures S2 and S3).

4.4 Evaluation of temperature return levels

The temperature return levels were categorized into 4 groups for both stationary and non-stationary cases: (a) between 30 and 35°C, (b) between 35 and 40°C, (c) between 40 and 45°C, and (d) between 45 and 50°C for all durations. Figure 8 compares how the number of grid points falling under each group of temperature varies for both S and NS conditions for 1-day duration, and similar representations for all other durations are given in the supplementary material (Figure S4). Majority of the grid points fall under the category of temperature between 40 and 45°C for all durations and return periods in both S and NS cases. It was found that the number of grid points falling into the category of 45 and 50°C increases when non-stationarity is considered and also with an increase in the return period. This increase was learned to be significantly gradual beyond the duration of 4 days. For instance, considering the sample grid point of Rajasthan (26.5 °N × 70.5 °E), the stationary temperature return level of 1-day duration for a 25-year return period (45.92°C) is almost equal to the non-stationary temperature return level of 1-day duration for a 10-year return period (45.98°C), which clearly indicates that the return period is decreasing while the return level is increasing when non-stationarity is considered.

A spatial interpolation is carried out in the QGIS platform using the derived temperature return levels of known 271 grid points in the S and NS frameworks to estimate temperatures at other unknown locations spanning all over India. Because of the high cost and limited resources, data collection is usually conducted only at a limited number of selected grid points. In this study, inverse distance weighted (IDW) interpolation technique is used to optimally estimate the temperatures at those locations where no samples or measurements were taken. The spatial interpolation was carried out for all durations and return periods to account for how the temperature varies all over India and its homogeneous regions. Figure 9 shows spatial interpolation carried out for 1-day duration for all return periods for both the S and NS cases. The spatially interpolated maps for all other durations are given in the supplementary material (Figures S5).

It is worth noting that the locations where temperature goes beyond 45°C are more when non-stationarity is considered. It can be clearly seen that as duration increases, the increase in temperature beyond 45°C is comparatively very gradual for both the S and NS cases. This proves that shorter-duration events display a larger temperature variation

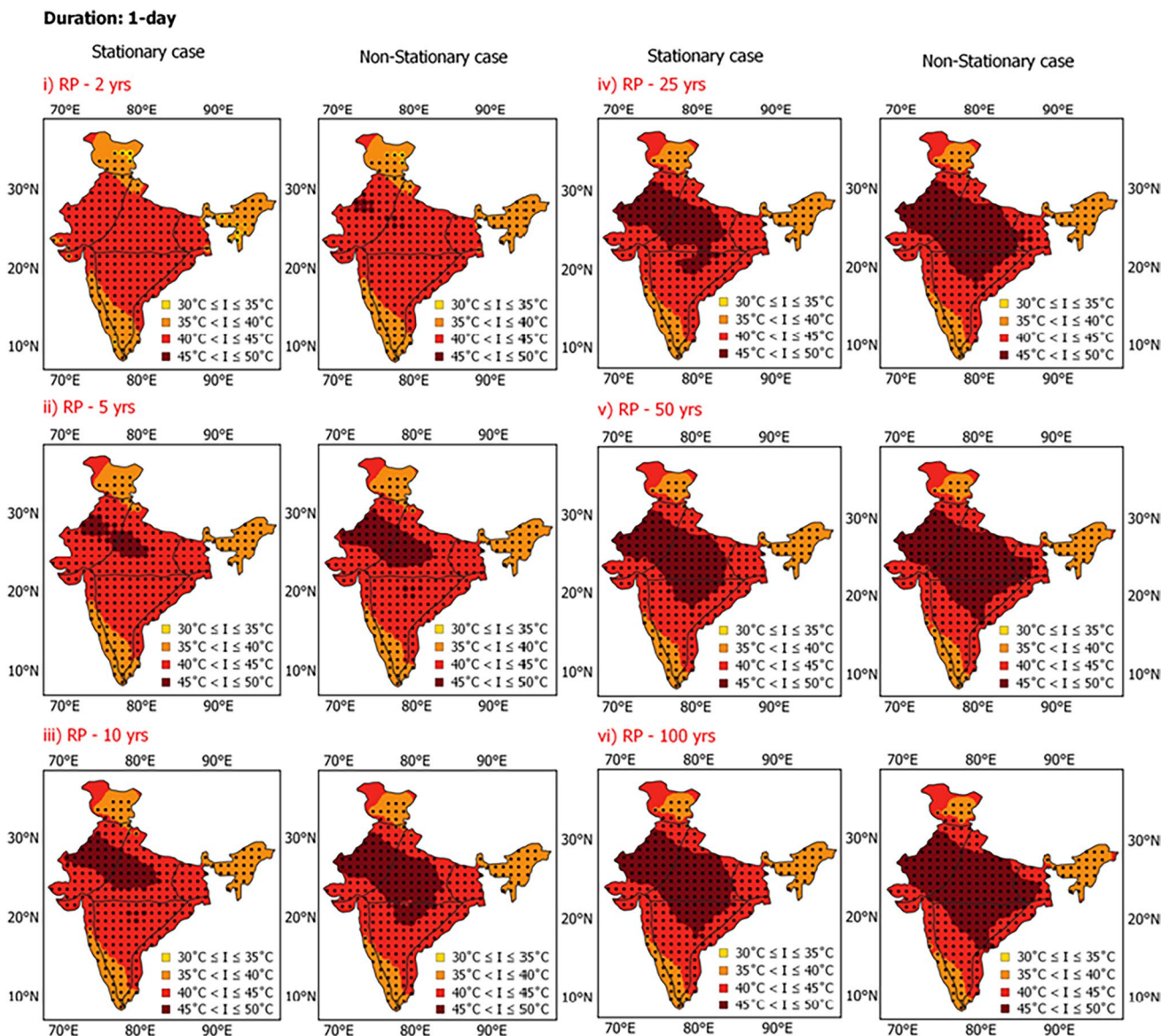


Fig. 9 Spatial interpolation of temperature intensities for 1-day duration

than longer-duration events. It was found that for shorter durations (1 day, 2 days, and 4 days), the NW, NC, and IP regions were highly affected by temperature increases of more than 45°C. Beyond the 4-day duration, the NW and NC regions were gradually affected by temperature increases above 45°C for all return periods. It can be concluded that the NW, NC, and IP regions require keen attention as they tend to have a temperature rise beyond 45°C earlier when compared to other regions. Ratnam et al. (2016) arrived at similar conclusions, such that heatwaves tend to occur mostly over the northwest and central parts of India. In addition, Mandal et al. (2019) specifically stated that the West and East Rajasthan, Punjab, Haryana, Chandigarh, Delhi, West Madhya Pradesh, West and East Uttar Pradesh,

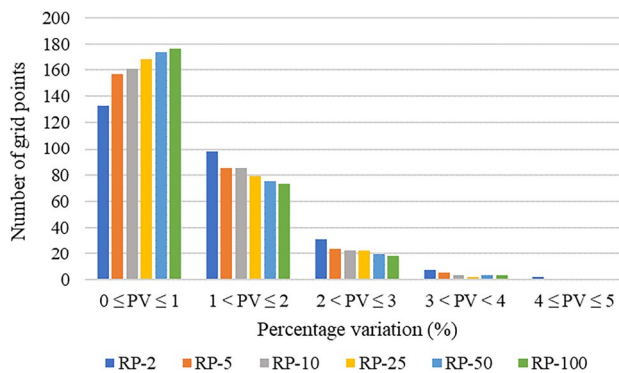


Fig. 10 Percentage variation of the grid points for 1-day duration

Chhattisgarh, Orissa, Vidarbha, and parts of Gangetic West Bengal, Coastal Andhra Pradesh, and Telangana experienced more than six heatwave days per year during the summer season (March, April, May, and June) in recent periods.

4.5 Percentage variation (PV)

As mentioned earlier, the non-stationary temperature estimates surpassed the stationary estimates for all durations and return periods. The percentage variation between S and NS temperature return levels was calculated for all durations. As an example, the PV for all grid points for 1-day duration is indicated in Fig. 10. The pictorial representation of PVs of all other durations is shown in the supplementary material (Figure S6). It was found that the majority of the grid points have a PV between 0 and 2%. A PV between 2 and 3% was observed for less than 30 grid points for all the return periods. A few grid points, say, less than 10, showed a PV varying from 3 to 5%. It can be highlighted that as the return period increases, the number of grid points with PV between 0 and 1% increases and the number of grid points with PV between 1 and 2% decreases.

The PV is also plotted spatially so as to visualize whether any definite pattern is observed in the PV in each temperature-homogeneous region. The illustration of PV in Fig. 11 and the supplementary material (Figure S7) gives a clear picture of the variation that occurred for each grid point during different return periods and durations. The grid points of WH, NW, NC, WC, EC, and IP have a PV of 0 to 3%. The majority of these grid points followed an analogous decreasing pattern in the PV for all durations in correspondence with the respective return periods. The grid points of the NE region displayed a heterogeneous category of PVs from 0 to 5% when compared with other regions. This indifferent pattern of PV in the NE region could be associated with the non-uniform best-fit models observed at each grid point. One grid point, 27.5° N × 88.5° E (Sikkim-NE), exhibited a continuous increase in PV for all durations and return periods, say, from 0.11°C for 1-day and 2-year RP to 1.7°C for 12-day and 100-year RP.

Majority of the grid points belonging to the NW, WH, WC, EC, NC, and IP regions showed a variation from 0% (0°C) to 2% (0.9°C) for all durations and return periods. Few grid points showed a variation from 2% (0.9°C) to 3%

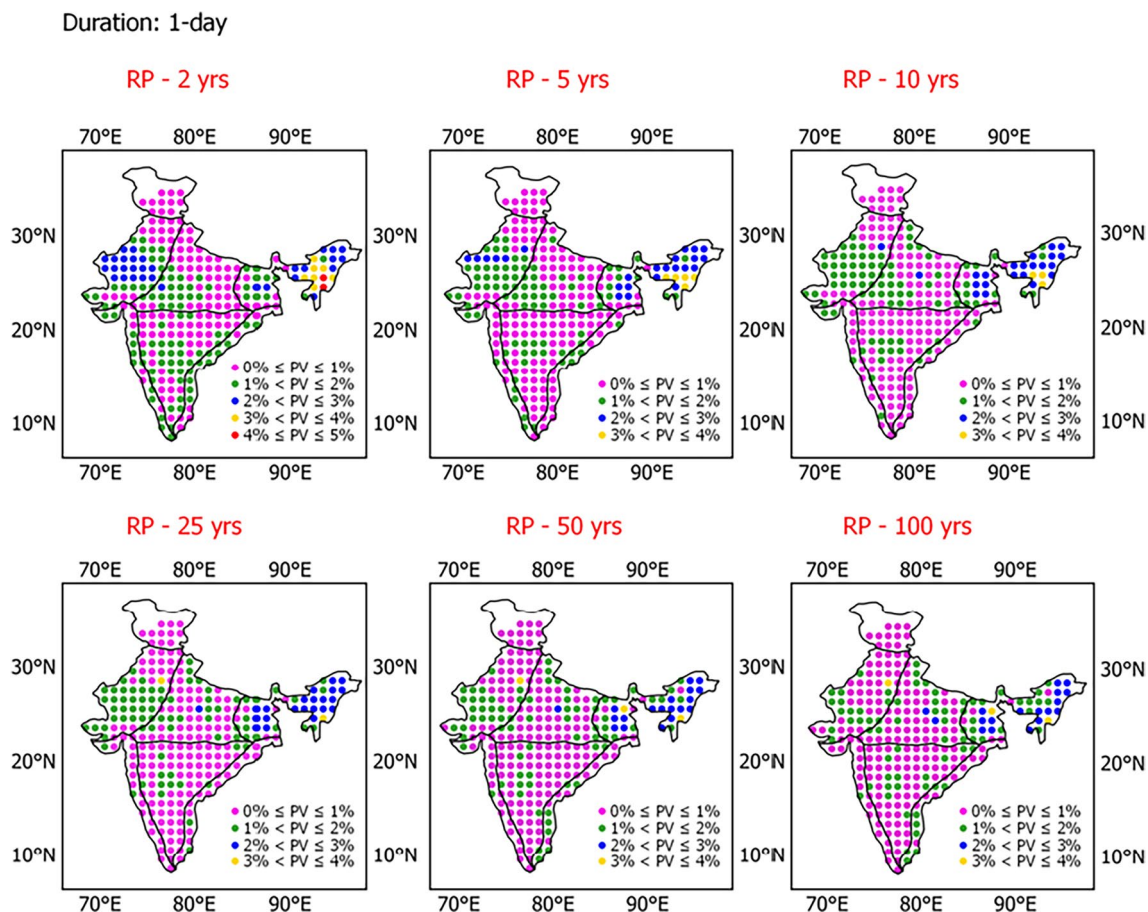


Fig. 11 Spatial representation of percentage variation for 1-day duration

(1.1°C) in the NW region for a shorter return period of 2 years. The NE region expressed a much higher temperature variation, upto 1.7°C for its selective grid points. India's average temperature has risen by around 0.7°C during the years 1901–2018 (Krishnan et al. 2020), which complements the findings from this study. In terms of India's temperature-homogeneous regions, it was observed that the NW, NC, and IP regions and parts of the EC, WC, and NE regions have a higher temperature (greater than 40°C) which is in line with the earlier findings (Dash and Mamgain 2011) that there is a significant increase in the maximum temperatures of the NW and southern Indian regions (EC, WC, and IP). Hence, these regions require more attention when considering events of extreme temperatures in the future.

5 Summary and conclusions

In this study, S and NS TDF analyses were carried out for the entire Indian subcontinent and its seven temperature-homogeneous regions to illustrate the significance of considering non-stationarity when developing TDF curves. IMD's historical (1° latitude × 1° longitude) gridded daily maximum temperature dataset of 271 grid points for a period of 1951–2019 was utilized for the study. The 1, 2, 4, 6, 8, 10, and 12 consecutive days of the annual maximum temperature time series (7 durations) were derived from the daily data. The results from the MK test showed that the number of grid points with an NS trend seemed to increase gradually from 57% for 1-day duration to 62% for 12-day duration. TDF modeling was done by building the S model and seven NS models, varying location and scale parameters linearly, quadratically, and exponentially with time as a covariate, along with their combinations. The best model for each duration temperature series is chosen based on AIC values, and the best fit GEV model is used for developing TDF relationships for various return periods of 2, 5, 10, 25, 50, and 100 years. The following conclusions can be drawn from this study:

(a) This study reveals that all the grid points exhibit significant non-stationarity in the distribution parameters. The goodness of fit is improved when using a NS approach with a time-dependent covariate when compared to the traditional S model for all durations. NS Model-1 was found to be the best model for around 55 to 67% of the grid points for all durations. About 20 to 25% of the remaining grid points had NS Model-6 as the best-fit model. From the homogeneous region-wise TDF analysis, it was learned that the WH, NW, NC, and WC regions have NS Model-1 as the best-fit model for majority of the grid points for all durations. The EC

and NE regions have NS Model-6 as the best-fit model for the majority of their grid points. Unlike EC, the NE region has NS Model-1 as the best model beyond a 6-day duration. IP region grid points have almost equal contributions to NS Model-1 and NS Model-6. It is evident that NS models based on location parameter varying linearly (NS Model-1) or quadratically (NS Model-6) with time improve the accuracy of NS TDF curves.

- (b) A comparison of stationary and non-stationary TDF curves for different return periods reveals that the stationary models underestimate the temperature return levels for all durations. This proves that considering the stationarity assumption while developing TDF curves will lead to the unexpected occurrence of heat waves, causing considerable damage to public health, infrastructure, and natural ecosystems. Ignoring the non-stationarity in the temperature return levels will drastically affect the shorter durations when compared to the longer durations. It was also noted that the return period decreases with an increase in return levels when non-stationarity is considered.
- (c) Majority of the grid points had a temperature return level between 40 and 45°C for all durations in both S and NS cases. As the return period increases, the number of grid points with temperatures between 45 and 50°C also increases. This increase was detected to be significantly gradual beyond the 4-day duration. The temperature-homogeneous regions, namely, NW, NC, and IP, were determined to be highly sensitive as they are prone to having higher temperatures above 45°C when compared to other regions.
- (d) The percentage variation between the S and NS temperature quantiles was calculated for all durations, and it was observed that the majority of the grid points had a variation from 0 to 2%. The number of grid points with PV between 0 and 1% increased as the return period increased. The PV is correlated with the best-fit model followed by a grid point, as the projected temperature return levels for all durations are computed using these models. The WH, NW, NC, WC, EC, and IP regions have a PV from 0 to 3% with a decreasing pattern as the return period increases for all durations. A higher PV from 2 to 5% was mainly seen in the NE region.

The findings of this study are solely based on time as a covariate, and this work can be further extended by introducing more covariates into the NS TDF modeling. Large-scale climatic oscillation indices were recognized as appropriate covariates when compared to time for developing IDF and QDF models as these indices have a direct relationship with rainfall and streamflow variability. The same might be applicable to TDF models as well, along with

other climatic drivers like solar irradiance, greenhouse gas emissions, clouds, fluxes, albedos, ozone, and water vapor. This demands the need for an extensive study to identify the suitable covariates for modeling TDF relationships. The selection of covariates is crucial, as they may have different effects on NS modeling for different geographical regions.

Supplementary Information The online version contains supplementary material available at <https://doi.org/10.1007/s00704-023-04606-x>.

Acknowledgements Meera G. Mohan acknowledges DST-SERB for the funding her fellowship. The authors wish to extend their gratitude to Indian Meteorological Department (IMD) for making their data resources available and free for access.

Author contribution All authors contributed to the idea conception. Meera. G. Mohan carried out the data collection, data preparation, and analysis and prepared the first draft of the manuscript. Adarsh S. played a supervisory role and helped in preparing the final version of the manuscript.

Funding This research work was supported by Science and Engineering Research Board, Department of Science and Technology (DST-SERB), Government of India (File Number: CRG/2021/003688).

Data availability The $1^{\circ} \times 1^{\circ}$ resolution daily maximum temperature data for India used in this study is freely available from the Indian Meteorological Department (IMD), Pune (<https://www.imdpune.gov.in/>).

Declarations

Competing interests The authors declare no competing interests.

References

- Adarsh S, Karthik S, Shyma M, Das PG, Shirin Parveen AT, Narayan S (2018) Developing short term drought severity-duration-frequency curves for Kerala meteorological subdivision, India using bivariate Copulas. *KSCE J Civ Eng* 22:962–973. <https://doi.org/10.1007/s12205-018-1404-9>
- Agilan V, Umamahesh NV (2017) What are the best covariates for developing non-stationary rainfall intensity-duration-frequency relationship? *Adv Water Resour* 101:11–22. <https://doi.org/10.1016/j.advwatres.2016.12.016>
- Cheng L, Gilleland E, Heaton MJ, AghaKouchak A (2014) Empirical Bayes estimation for the conditional extreme value model. *Stat* 3(1):391–406. <https://doi.org/10.1002/sta4.71>
- Coles S (2001) An introduction to statistical modelling of extreme values. Springer, New York
- Dash SK, Mamgain A (2011) Changes in the frequency of different categories of temperature extremes in India. *J Appl Meteor Clim* 50(9):1842–1858. <https://doi.org/10.1175/2011JAMC2687.1>
- De US, Mukhopadhyay RK (1998) Severe heat wave over the Indian subcontinent in 1998, in perspective of global climate. *Curr Sci* 75:1308–1315 <https://www.jstor.org/stable/24101015>
- De US, Dube RK, Rao GSP (2005) Extreme weather events over India in last 100 years. *J Ind Geophys Union* 9(3):173–187
- Devi R, Gouda KC, Lenka S (2021) Temperature-duration-frequency analysis over Delhi and Bengaluru city in India. *Theoret Appl Climatol* 147:291–305. <https://doi.org/10.1007/s00704-021-03824-5>
- Douglas EM, Vogel RM, Kroll CN (2000) Trends in floods and low flows in the United States: impact of spatial correlation. *J Hydrol* 240(1–2):90–105. [https://doi.org/10.1016/S0022-1694\(00\)00336-X](https://doi.org/10.1016/S0022-1694(00)00336-X)
- El Adlouni S, Ouarda TBMJ, Zhang X, Roy R, Bobee B (2007) Generalized maximum likelihood estimators for the nonstationary generalized extreme value model. *Water Resour Res* 43(3):W03410. <https://doi.org/10.1029/2005WR004545>
- Ghasemi AR (2015) Changes and trends in maximum, minimum and mean temperature series in Iran. *Atmos Sci Lett* 16(3):366–372. <https://doi.org/10.1002/asl2.569>
- Gumbel EJ (1958) Statistics of extremes. Dover Publications, Mineola, NY, USA
- Hosking JRM, Wallis JR, Wood EF (1985) Estimation of the generalized extreme-value distribution by the method of probability weighted moments. *Technometrics* 27:251–261. <https://doi.org/10.1080/00401706.1985.10488049>
- Hosking JRM (1990) L-moments: analysis and estimation of distributions using linear combinations of order statistics. *J R Statist Soc B* 52:105–124. <https://doi.org/10.1111/j.2517-6161.1990.tb01775.x>
- IPCC (2013) In: Stocker TF, Qin D, Plattner G-K, Tignor M, Allen SK, Boschung J, Nauels A, Xia Y, Bex V, Midgley PM (eds) Summary for policymakers. In: Climate change 2013: the physical science basis. Contribution of Working Group I to the Fifth Assessment Report of the Intergovernmental Panel on Climate Change. Cambridge University Press, Cambridge, United Kingdom and New York, NY, USA
- IPCC (2021) Climate Change 2021: The Physical Science Basis. In: Masson-Delmotte V, Zhai P, Pirani A, Connors SL, Péan C, Berger S, Caud N, Chen Y, Goldfarb L, Gomis MI, Huang M, Leitzell K, Lonnoy E, Matthews JBR, Maycock TK, Waterfield T, Yelekçi O, Yu R, Zhou B (eds) Contribution of Working Group I to the Sixth Assessment Report of the Intergovernmental Panel on Climate Change. Cambridge University Press, United Kingdom and New York, NY, USA, p 2391. <https://doi.org/10.1017/9781009157896>
- Javelle P, Ouarda TBMJ, Lang M, Bobée B, Galéa G, Grésillon JM (2002) Development of regional flood-duration-frequency curves based on the index-flood method. *J Hydrol* 258(1):249–259. [https://doi.org/10.1016/S0022-1694\(01\)00577-7](https://doi.org/10.1016/S0022-1694(01)00577-7)
- Katz RW, Parlange MB, Naveau P (2002) Statistics of extremes in hydrology. *Adv Water Resour* 25:1287–1304. [https://doi.org/10.1016/S0309-1708\(02\)00056-8](https://doi.org/10.1016/S0309-1708(02)00056-8)
- Kendall MG (1975) Rank correlation methods, 4th edn. Charles Griffin, London
- Khalik MN, St-Hilaire A, Ouarda TBMJ, Bobée B (2005) Frequency analysis and temporal pattern of occurrences of southern Quebec heatwaves. *Int J Climatol* 25:485–504. <https://doi.org/10.1002/joc.1141>
- Khan A, Chatterjee S, Bisai D (2015) On the long-term variability of temperature trends and changes in surface air temperature in Kolkata Weather Observatory, West Bengal, India. *Meteorology Hydrol Wat Manage* 3(2):1–15
- Khan N, Shahid S, Ismail T et al (2019) Trends in heat wave related indices in Pakistan. *Stoch Environ Res Risk Assess* 33:287–302. <https://doi.org/10.1007/s00477-018-1605-2>
- Kothawale DR, Rupa Kumar K (2005) On the recent changes in surface temperature trends over India. *Geophys Res Lett* 32(18). <https://doi.org/10.1029/2005GL023528>
- Kothawale DR, Revadekar JV, Kumar KR (2010) Recent trends in pre-monsoon daily temperature extremes over India. *J Earth Syst Sci* 119(1):51–65. <https://doi.org/10.1007/s12040-010-0008-7>
- Krishnan R et al (2020) Introduction to climate change over the Indian region. In: Krishnan R, Sanjay J, Gnanaseelan C, Mujumdar M, Kulkarni A, Chakraborty S (eds) Assessment of climate change

- over the Indian region. Springer, Singapore. https://doi.org/10.1007/978-981-15-4327-2_1
- Madsen H, Rasmussen PF, Rosbjerg D (1997) Comparison of annual maximum series and partial duration series methods for modelling extreme hydrologic events: 1. At- site modeling. *Wat Resour Res* 33(4):747–758. <https://doi.org/10.1029/96WR03848>
- Mandal R, Joseph S, Sahai AK et al (2019) Real time extended range prediction of heat waves over India. *Sci Rep* 9:9008. <https://doi.org/10.1038/s41598-019-45430-6>
- Mann HB (1945) Non-parametric tests against trend. *Econometrica* 13:163–171
- Mazdiyasi O, AghaKouchak A, Davis SJ, Madadgar S, Mehran A, Ragno E, Sadegh M, Sengupta A, Ghosh S, Dhanya CT, Niknejad M (2017) Increasing probability of mortality during Indian heat waves. *Sci Adv* 3(6). <https://doi.org/10.1126/sciadv.1700066>
- Mazdiyasi O, Sadegh M, Chiang F et al (2019) Heat wave intensity duration frequency curve: a multivariate approach for hazard and attribution analysis. *Sci Rep* 9:14117. <https://doi.org/10.1038/s41598-019-50643-w>
- Mondal A, Mujumdar PP (2015) Modelling non-stationarity in intensity, duration and frequency of extreme rainfall over India. *J Hydrol* 521:217–231. <https://doi.org/10.1016/j.jhydrol.2014.11.071>
- Onyutha C, Willems P (2013) Uncertainties in flow-duration-frequency relationships of high and low flow extremes in Lake Victoria basin. *Water* 5(4):1561–1579. <https://doi.org/10.3390/w5041561>
- Ouarda TBMJ, Charron C (2018) Nonstationary temperature-duration-frequency curves. *Sci Rep* 8(1):15493. <https://doi.org/10.1038/s41598-018-33974-y>
- Oza M, Kishtawal CM (2015) Spatio-temporal changes in temperature over India. *Curr Sci* 109(6):1154–1158. <https://doi.org/10.18520/v109/i6/1154-1158>
- Pai DS, Thapliyal V, Kokate PD (2004) Decadal variation in the heat and cold waves over India during 1971–2000. *Mausam* 55:281–292. <https://doi.org/10.54302/mausam.v55i2.1083>
- Perkins SE, Alexander LV (2013) On the measurement of heat waves. *J Climate* 26(13):4500–4517. <https://doi.org/10.1175/JCLI-D-12-00383.1>
- Raghavan K (1966) A climatological study of severe heat waves in India. *Mausam* 17(4):581–586. <https://doi.org/10.54302/mausam.v17i4.5760>
- Rahmat SN, Jayasuriya N, Bhuiyan M (2015) Development of drought severity duration-frequency curves in Victoria. Australia *Austral J Wat Res* 19(2):156–160. <https://doi.org/10.1080/13241583.2016.1176779>
- Rao GSP, Murthy MK, Joshi UR (2005) Climate change over India as revealed by critical extreme temperature analysis. *Mausam* 56:601–608. <https://doi.org/10.54302/mausam.v56i3.990>
- Ratnam J, Behera S, Ratna S et al (2016) Anatomy of Indian heatwaves. *Sci Rep* 6:24395. <https://doi.org/10.1038/srep24395>
- Ray LK, Goel NK (2019) Non-stationary frequency analysis of extreme rainfall events across India. *J Hydrol Eng* 24:(8)
- Renima M, Remaoun M, Boucefiane AASB (2018) Regional modelling with flood-duration-frequency approach in the middle Cheliff watershed. *J Wat and Land Develop* 36(1):129–141. <https://doi.org/10.2478/jwld-2018-0013>
- Revadekar JV, Kothawale DR, Patwardhan SK (2012) About the observed and future changes in temperature extremes over India. *Nat Hazards* 60:1133–1155. <https://doi.org/10.1007/s11069-011-9895-4>
- Rohini P, Rajeevan M, Srivastava AK (2016) On the variability and increasing trends of heat waves over India. *Sci Rep* 6:1–9. <https://doi.org/10.1038/srep26153>
- Roy SS (2019) Spatial patterns of trends in seasonal extreme temperatures in India during 1980–2010. *Weath Clim Ext* 24:100203. <https://doi.org/10.1016/j.wace.2019.100203>
- Shiau JT, Modarres R (2009) Copula-based drought severity-duration-frequency analysis in Iran. *Meteorol Appl* 16(4):481–489. <https://doi.org/10.1002/met.145>
- Singh S, Mall RK, Singh N (2020) Changing spatio-temporal trends of heat wave and severe heat wave events over India: an emerging health hazard. *Int J Climatol* 18(5):E1831–E1845. <https://doi.org/10.1002/joc.6814>
- Smith RL (1985) Maximum likelihood estimation in a class of non-regular cases. *Biometrika* 72:67–90. <https://doi.org/10.2307/2336336>
- Sonali P, Nagesh Kumar D (2013) Review of trend detection methods and their application to detect temperature change in India. *J Hydrol* 476:212–227. <https://doi.org/10.1016/j.jhydrol.2012.10.034>
- Srivastava AK, Rajeevan M, Kshirsagar SR (2009) Development of high resolution daily gridded temperature data set (1969–2005) for the Indian region. *Atmos Sci Lett* 10(4):249–254. <https://doi.org/10.1002/asl.232>
- Sung JH, Chung ES (2014) Development of streamflow drought severity–duration–frequency curves using the threshold level method. *Hydrol Earth Syst Sci* 18:3341–3351. <https://doi.org/10.5194/hess-18-3341-2014>
- Tank AMGK, Können GP (2003) Trends in indices of daily temperature and precipitation extremes in Europe, 1946–1999. *J Climate* 16:3665–3680. [https://doi.org/10.1175/1520-0442\(2003\)016<3665:THODT>2.0.CO;2](https://doi.org/10.1175/1520-0442(2003)016<3665:THODT>2.0.CO;2)
- Vinnarasi R, Dhanya CT, Chakravorthy A, Aghakouchak A (2017) Unravelling diurnal asymmetry of surface temperature in different climate zones. *Sci Rep* 7. <https://doi.org/10.1038/s41598-017-07627-5>
- Yan Z, Jones PD DTD, Moberg A, Bergström H, Camuffo D, Cocheo C, Maugeri M, Demarée GR, Verhoeve T, Thoen E BM, Rodríguez R, Martiín-Vide J, Yang C (2002) Trend of extreme temperatures in Europe and China based on daily observations. *Clim Change* 53:355–392. <https://doi.org/10.1023/A:1014939413284>

Publisher's note Springer Nature remains neutral with regard to jurisdictional claims in published maps and institutional affiliations.

Springer Nature or its licensor (e.g. a society or other partner) holds exclusive rights to this article under a publishing agreement with the author(s) or other rightsholder(s); author self-archiving of the accepted manuscript version of this article is solely governed by the terms of such publishing agreement and applicable law.